JACS
JOURNAL OF THE AMERICAN CHEMICAL SOCIETY

Communication

pubs.acs.org/JACS

Synthesis of Gold Hexagonal Bipyramids Directed by Planar-Twinned Silver Triangular Nanoprisms

Michelle L. Personick, Mark R. Langille, Jinsong Wu, and Chad A. Mirkin*

Department of Chemistry, Department of Materials Science and Engineering, and International Institute for Nanotechnology, Northwestern University, 2145 Sheridan Road, Evanston, Illinois 60208, United States

Supporting Information

ABSTRACT: The direct growth of planar-twinned Au nanoparticles (NPs) in high yield remains a challenge in shape-controlled NP synthesis largely because suitable planar-twinned seeds for Au NP growth have not been identified to date. Herein we describe the use of planar-twinned Ag triangular nanoprisms as a means to dictate Au NP twin structure. In a one-pot process, the Ag triangular nanoprisms first undergo oxidative Au replacement, forming Ag–Au alloy nanoframes and concomitantly releasing Ag^+ into solution, which then directs subsequent Au NP growth through an underpotential deposition process. The planar-twinned structure of the initial Ag nanoprism is maintained throughout particle growth. Using this method, we have successfully synthesized Au hexagonal bipyramids in high yield for the first time.

Methods for deliberately controlling the size and shape of noble-metal nanoparticles (NPs) are necessary for optimally harnessing their emergent physical and chemical properties.[1−6] Of these two parameters, shape is often more difficult to tailor deliberately, and as a result, a large amount of recent research has focused on shape control of noble-metal NPs, leading to the design of growth conditions that favor the formation of NPs with particular surface facets.[1,7−15] However, NP shape is dictated not only by facets but also by twin structure (single-crystalline, planar-twinned, or multiply twinned), and thus, selective production of NPs with a specific twin structure is also important.[16−18] Xia and co-workers showed that for Ag NPs it is possible to control twin structure through selective etching processes.[1] In another example, Xu and co-workers reported a high-yield synthesis of single-crystalline Au NPs using single-crystalline seeds to initiate growth.[19] However, analogous syntheses have not been developed for the direct synthesis of planar-twinned Au nanostructures, such as right bipyramids and bitetrahedra. The vast majority of syntheses to date produce planar-twinned Au NPs concomitantly with single-crystalline NPs. For example, twinned right bipyramids are a minor product of the reaction conditions used to generate single-crystalline Au nanocubes,[20] and while twinned {110}-faceted bipyramids can be prepared, they are formed in the presence of single-crystalline rhombic dodecahedra.[21]

In some syntheses, the twinned products can be separated via filtration or through other differential separation methods.[21−23] In other cases, such as when the single-crystalline and twinned products have similar sizes or the desired twinned product is formed in very low yield relative to the other products, such separation is not possible. However, the properties of twinned NPs may be more attractive for particular applications than those of their single-crystalline counterparts, such as the significantly red-shifted resonances of highly anisotropic planar-twinned NPs, which can be tuned far into the IR.[21,22,24] While it is known that NP twin structure can be dictated through the use of twinned seeds,[1] no suitable planar-twinned seeds have been identified to date for use in the direct synthesis of planar-twinned Au NPs. Herein we report a novel way to achieve control of twin structure by using planar-twinned Ag triangular nanoprisms as twinned seeds in a seed-mediated aqueous synthesis of Au NPs.

We previously observed the growth of Au hexagonal bipyramids as a minor product (~5% yield) in the synthesis of tetrahexahedral (THH) Au NPs (Figure S1 in the Supporting Information). We show herein that seeding a reaction with the desired planar-twin structure increases the yield of these planar-twinned NPs, allowing these unusual high-index structures to be prepared in high yield (>85%) for the first time (Figure 1). We

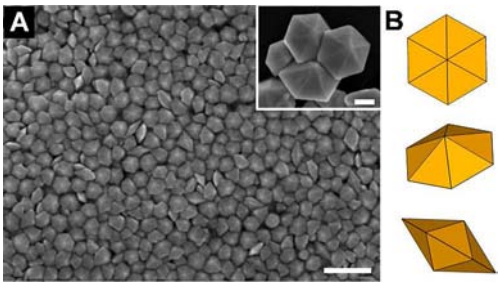

Figure 1. (A) Low-magnification scanning electron microscopy (SEM) image of Au hexagonal bipyramids and (inset) high-magnification SEM image of larger hexagonal bipyramids. Scale bars: 200 nm and (inset) 100 nm. (B) Models of hexagonal bipyramids viewed at different angles.

show that the Ag nanoprisms are first partially exchanged with Au via either galvanic replacement[25] or the Kirkendall effect[26] to form Ag–Au alloy nanoframes, which then undergo further oxidative Au replacement and Au overgrowth to form Au hexagonal bipyramids, a shape previously accessible only in low yields.[27] During the latter stages of growth, the shape of the bipyramids is controlled by an underpotential deposition (UPD) process involving the Ag^+ ions produced in situ as a result of the

Received: January 23, 2013
Published: March 1, 2013

 © 2013 American Chemical Society dx.doi.org/10.1021/ja400794q | J. Am. Chem. Soc. 2013, 135, 3800−3803

oxidative replacement of Ag by Au^+ earlier in the reaction (Scheme 1).

Scheme 1. Synthesis of Au Hexagonal Bipyramids

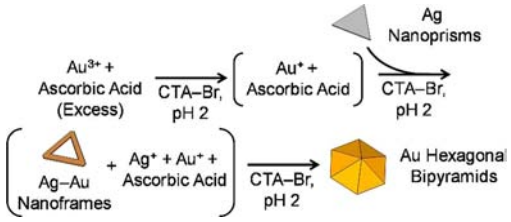

Ag triangular nanoprisms with an edge length of ~50 nm were synthesized via a previously published plasmon-mediated synthesis (see Figure 2A).[2,3,28] In this method, small spherical Ag NPs are irradiated with visible light (550 nm) and serve as plasmonic seeds. Oxidation of a population of the seed particles by O_2 provides a source of Ag^+, and the visible-light irradiation drives plasmonic excitation of the seeds as well as the subsequent citrate reduction of Ag^+ to Ag^0, which is deposited onto the remaining seed particles.[29−32] In addition, the interaction of the incident light with the plasmon resonance of the growing Ag NPs provides a means of controlling the size of the final prisms, which stop growing after their plasmon resonances become red-shifted from the excitation wavelength, leading to size focusing of the NP product.[28]

In a typical synthesis, 10.0 mL of Ag nanoprisms were centrifuged and concentrated to a volume of ~150.0 μL in H_2O and subsequently used to seed the growth of the Au hexagonal bipyramids. The origin of the Ag prism seeds was not critical, as Ag nanoprisms generated via a thermal method[33] could also be used as seeds (Figure S2). The size of the hexagonal bipyramids could be controlled by varying the amount of prism seeds added (Figures 1A, S2, and S3). A growth solution was prepared by sequentially adding 0.1 mL of 1 M HCl, 0.25 mL of 10 mM $HAuCl_4$, and 50.0 μL of 100 mM ascorbic acid to 5.0 mL of 100 mM cetyltrimethylammonium bromide (CTA-Br). The reaction was initiated by the addition of the Ag nanoprism seeds (above) to the growth solution, which was mixed gently and kept at 30 °C in a water bath for the duration of the reaction (~2 h).

The evolution of the Ag triangular nanoprisms into Au hexagonal bipyramids was monitored by taking samples of the growth solution 0, 1, 5, and 10 min after the addition of the Ag nanoprisms as well as at reaction completion. The reaction was quenched with bis(*p*-sulfonatophenyl)phenylphosphine dihydrate potassium salt, which binds to excess Au^+ ions and the Au particle surface and inhibits further particle growth.[34−36] High-angle annular dark-field scanning transmission electron microscopy (HAADF-STEM) images and energy-dispersive X-ray spectroscopy (EDS) elemental maps of NPs during early growth stages (0−1 min) show the oxidative replacement of Ag in the triangular nanoprisms by Au^+ ions to generate Ag−Au alloy nanoframes, as expected on the basis of literature precedents and the greater nobility of Au relative to Ag (Figures 2B,C, S4, and S5).[25,37−39] As the reaction proceeds, the frames begin to fill in with Au, forming structures that are more solid than the preceding frames (Figure 2D). The partially filled frames then grow into the hexagonal bipyramid structures, although the frames are still visible in the interiors of the bipyramids in the HAADF-STEM image (Figure 2E). Finally, the hexagonal bipyramids continue to grow larger and the frames become less apparent because of the increased amount of material around the frame (Figures 2F and S6).

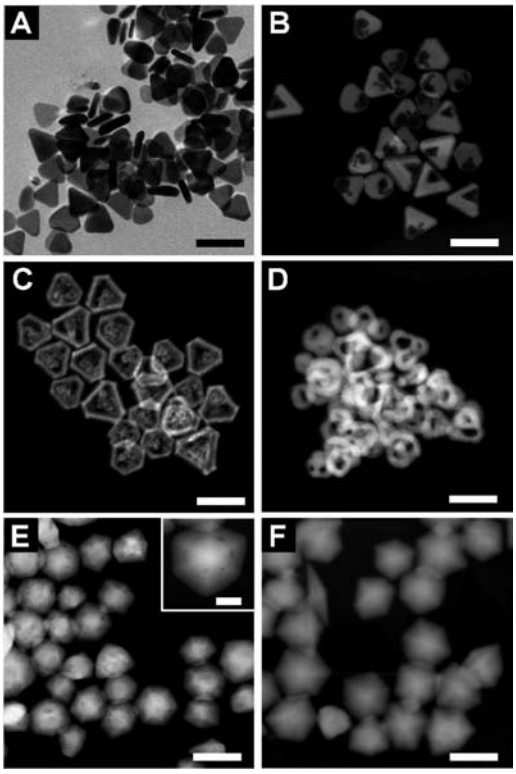

Figure 2. (A) TEM image of the as-synthesized Ag triangular nanoprisms. (B−F) HAADF-STEM images of the growth of Au hexagonal bipyramids at selected time points over the course of the reaction: (B) 0 min (i.e., immediately after the addition of nanoprisms); (C) 1 min; (D) 5 min; (E) 10 min; (F) ~2 h (reaction completion). Scale bars: 100 nm. Inset in (E): high-magnification HAADF-STEM image of a single hexagonal bipyramid. Scale bar: 25 nm.

The hexagonal bipyramid shape is related to that of THH NPs[40−42] reported in the literature in that the sixfold symmetry of the hexagonal bipyramid shape resembles that of a corner of a single-crystalline THH NP (Figure 3). This is analogous to the case of the planar-twinned {110}-faceted bipyramids we reported previously, whose structure resembles the threefold-symmetric corner of a single-crystalline {110}-faceted rhombic dodecahedron (Figure S7).[21] In addition, we occasionally observed hexagonal bipyramids as a minor side product of the THH NP synthesis (Figure S1). The similarity of the hexagonal bipyramid and THH shapes led us to predict that we could produce the bipyramids in high yield if we began with planar-twinned seeds and used the growth conditions which lead to the formation of THH NPs (Scheme S1). The THH shape is controlled by Ag UPD, a process by which a monolayer or submonolayer of Ag can

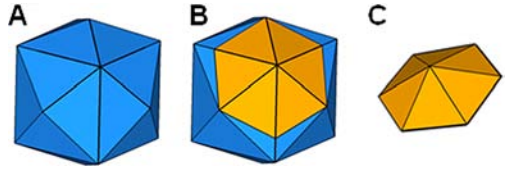

Figure 3. Models showing the shape relationship between tetrahexahedra and hexagonal bipyramids: (A) THH particle; (B) THH particle with a sixfold-symmetric corner highlighted; (C) hexagonal bipyramid.

dx.doi.org/10.1021/ja400794q | *J. Am. Chem. Soc.* 2013, 135, 3800−3803

be deposited onto an existing Au surface at a positive potential relative to the Nernst potential of Ag.[7,8,43−46] Under the low-pH conditions of the THH NP synthesis, ascorbic acid is not a strong enough reducing agent to reduce Ag^+ in bulk, so Ag deposition occurs via UPD onto the surface of the growing Au NPs occurs via UPD. The The Ag^+ reduced in this manner is preferentially deposited onto more open Au facets, which possess a greater number of low-coordinated Au atoms than other facets, thus stabilizing these surfaces and passivating them toward further Au deposition.[7]

On the basis of this understanding of the surface chemistry that controls the growth of THH NPs, we designed synthetic conditions for the hexagonal bipyramids that are nearly identical to those used to produce THH NPs in terms of reagents used, reagent concentrations, and pH.[41] One notable difference is the absence of the key shape-directing agent, Ag^+, in the hexagonal bipyramid growth solution. However, the exchange of Ag in the nanoprisms with Au^+ ions generates Ag^+ ions in situ, which can then be deposited onto the surface of the growing bipyramids via UPD, just as Ag^+ ions added to the growth solution do in the case of the THH NPs. The total calculated amount of Ag in the hexagonal bipyramid growth solution (due to added Ag nanoprisms) is ∼0.15 mM, which is close to the concentration of Ag^+ in the THH NP synthesis (0.1 mM).[41] Because the Ag nanoprisms are not completely converted to Ag^+ ions, the Ag^+ concentrations in the two reaction solutions should be similar. To confirm the occurrence of UPD, X-ray photoelectron spectroscopy (XPS) was used to determine the Ag/Au ratio on the surface of the final hexagonal bipyramids for comparison with the ratio for THH NPs (Figure S8). These Ag/Au ratios were expected to be similar because of the nearly identical reaction conditions and the related shapes of the two particle types, and this was confirmed by the experimental Ag/Au ratios of 0.18 for the hexagonal bipyramids and 0.17 for the THH NPs (the latter value is in accordance with the surface Ag/Au ratio we reported previously[8]). The similarity of the surface Ag/Au ratios for the hexagonal bipyramids and THH NPs provides strong evidence that surface passivation by Ag UPD occurs and plays the same role in the formation of these two structures.

The analogy between the shapes of the hexagonal bipyramids and THH NPs suggests that the hexagonal bipyramids should be bound by facets similar to those of the THH NPs and should contain a planar twin boundary. These two hypotheses regarding the structure of the hexagonal bipyramids were probed using transmission electron microscopy (TEM). Precise determination of the indices of the facets of the hexagonal bipyramids is challenging because the high symmetry of the bipyramids results in very similar TEM projections for a variety of different NP orientations. This similarity makes it difficult to define the orientation of the bipyramids relative to the electron beam, which in turn prevents the collection of conclusive electron diffraction (ED) patterns directly from their facets. An alternative method of assigning Miller indices is to use ED to determine the crystallographic directions of the equatorial and radial edges of the bipyramids and then to calculate the plane that contains both edges. We considered the equatorial edges to be those defining the hexagon and the radial edges to be those radiating from the sixfold-symmetric vertex of the bipyramids. To determine the crystallographic direction of the equatorial edges, the hexagonal bipyramids were oriented to the [111] zone axis. This placed the equatorial edges perpendicular to the electron beam, resulting in a hexagonal projection (Figure 1B, top model, and Figure S9A). The direction of the equatorial edges was then determined from their orientation with respect to the [111] nano-ED pattern of the bipyramid by superimposing the lines defined by the edges onto the diffraction pattern (Figure S9), which showed that the equatorial edges lie along the ⟨211⟩ crystallographic directions of the fcc unit cell. Using the same technique, we then analyzed the direction of the radial edges of the bipyramid by orienting a particle to the [110] zone axis (Figures 4A,B, S10, and S11). In

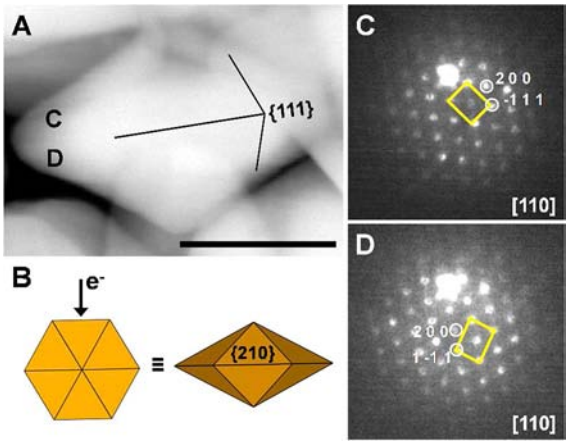

Figure 4. (A) HAADF-STEM image of a single hexagonal bipyramid oriented to the [110] zone axis with the top and bottom halves of the crystal labeled and three {111} planes annotated. Scale bar: 50 nm. (B) Models of the orientation of the particle shown in (A). The arrow indicates the orientation of the electron beam with respect to the particle. (C, D) Nano-ED patterns obtained from the (C) top and (D) bottom halves of the particle in (A). ⟨111⟩ diffraction spots are connected by yellow lines to indicate the relative orientations of the diffraction patterns.

this orientation, four of the radial edges of the bipyramid were perpendicular to the electron beam and thus were projected as lines, whose crystallographic directions were determined to be ⟨100⟩ and ⟨221⟩ by their orientations relative to the [110] nano-ED pattern. Separate calculations of the plane containing each of these axial edge directions and the equatorial edge direction (⟨211⟩) and of the plane containing both axial edges showed that the planes of the facets of the hexagonal bipyramid are {210}. In addition, the theoretical angle between a {210} facet and the (111) plane is 39°, which matches well with the experimentally measured angle of ∼37° between the facets and the proposed location of the {111} twin plane. Therefore, while the facets of the hexagonal bipyramids are not exactly identical to those of the THH NPs, they are high-index facets. Furthermore, the {210} facets are closely related to the {730} facets of THH NPs because {730} facets are composed of two {210} steps and one {310} step.

To validate the second hypothesis that the use of planar-twinned Ag seeds would lead to the formation of planar-twinned products, we were able to confirm the presence of a planar twin in the product bipyramids via nano-ED. Single hexagonal bipyramids were oriented to the [110] zone axis, in which the {111} twin plane of the bipyramid, if present, would be parallel to the electron beam (Figures 4A,B and S10). With the hexagonal bipyramid oriented in this way, we obtained nano-ED patterns from the top and bottom halves of the bipyramid and compared their relative orientations (Figure 4C,D). Using the ⟨111⟩ diffraction spots as a guide (connected with yellow lines in Figure 4C,D) we determined that the two [110] diffraction patterns had mirror symmetry with respect to one another, indicating the

dx.doi.org/10.1021/ja400794q | J. Am. Chem. Soc. 2013, 135, 3800−3803

presence of a twin plane between the top and bottom sections of the crystal. The {111} lattice planes in the twin crystals of the bipyramids (determined from the ED data) are illustrated in Figure 4A, confirming that the twin is the typical {111} twin of an fcc crystal. This demonstrates that the twin plane of the Ag nanoprism seeds was indeed maintained during the oxidative Au replacement and growth processes.

In conclusion, we have reported a method for using planar-twinned Ag triangular nanoprisms as novel seeds for the synthesis of planar-twinned Au hexagonal bipyramids. Importantly, this method points toward the potential use of these triangular nanoprism seeds in a more general manner to facilitate the synthesis of other planar-twinned NPs that currently cannot be prepared in high yield, such as bitetrahedra and right bipyramids.

■ ASSOCIATED CONTENT

Supporting Information

Experimental details and additional data. This material is available free of charge via the Internet at http://pubs.acs.org.

■ AUTHOR INFORMATION

Corresponding Author

chadnano@northwestern.edu

Notes

The authors declare no competing financial interest.

■ ACKNOWLEDGMENTS

This work was supported by AFOSR Awards FA9550-11-1-0275, FA9550-12-1-0280, and FA9550-09-1-0294; DoD/NSSEFF/NPS Award N00244-09-1-0012; the NU Nonequilibrium Energy Research Center (NERC) DOE Award DE-SC0000989; Nanoscale Science and Engineering Initiative NSF Award EEC-0647560; NSF MRSEC Awards DMR-0520513 and DMR-1121262; and shared facilities at the Materials Research Center. Microscopy work was performed in the EPIC Facility of the NU*ANCE* Center, which is supported by NSF-NSEC, NSF-MRSEC, the Keck Foundation, the State of Illinois, and NU. XPS experiments were performed at the Keck-II facilities at NU. M.L.P. gratefully acknowledges support from the DoD through the National Defense Science & Engineering Graduate Fellowship Program (32 CFR 168a) and from the NSF through a Graduate Research Fellowship.

■ REFERENCES

(1) Xia, Y.; Xiong, Y.; Lim, B.; Skrabalak, S. E. *Angew. Chem., Int. Ed.* **2009**, *48*, 60.
(2) Jin, R.; Cao, Y.; Mirkin, C. A.; Kelly, K. L.; Schatz, G. C.; Zheng, J. G. *Science* **2001**, *294*, 1901.
(3) Jin, R.; Cao, Y. C.; Hao, E.; Métraux, G. S.; Schatz, G. C.; Mirkin, C. A. *Nature* **2003**, *425*, 487.
(4) Jones, M. R.; Osberg, K. D.; Macfarlane, R. J.; Langille, M. R.; Mirkin, C. A. *Chem. Rev.* **2011**, *111*, 3736.
(5) Zhou, K.; Li, Y. *Angew. Chem., Int. Ed.* **2012**, *51*, 602.
(6) Giljohann, D. A.; Seferos, D. S.; Daniel, W. L.; Massich, M. D.; Patel, P. C.; Mirkin, C. A. *Angew. Chem., Int. Ed.* **2010**, *49*, 3280.
(7) Personick, M. L.; Langille, M. R.; Zhang, J.; Mirkin, C. A. *Nano Lett.* **2011**, *11*, 3394.
(8) Langille, M. R.; Personick, M. L.; Zhang, J.; Mirkin, C. A. *J. Am. Chem. Soc.* **2012**, *134*, 14542.
(9) Tao, A. R.; Habas, S.; Yang, P. *Small* **2008**, *4*, 310.
(10) Wu, H.-L.; Kuo, C.-H.; Huang, M. H. *Langmuir* **2010**, *26*, 12307.
(11) Wiley, B.; Sun, Y.; Chen, J.; Cang, H.; Li, Z.-Y.; Li, X.; Xia, Y. *MRS Bull.* **2005**, *30*, 356.
(12) Rycenga, M.; Cobley, C. M.; Zeng, J.; Li, W.; Moran, C. H.; Zhang, Q.; Qin, D.; Xia, Y. *Chem. Rev.* **2011**, *111*, 3669.
(13) Nikoobakht, B.; El-Sayed, M. A. *Chem. Mater.* **2003**, *15*, 1957.
(14) Jana, N. R.; Gearheart, L.; Murphy, C. J. *J. Phys. Chem. B* **2001**, *105*, 4065.
(15) Grzelczak, M.; Pérez-Juste, J.; Mulvaney, P.; Liz-Marzán, L. M. *Chem. Soc. Rev.* **2008**, *37*, 1783.
(16) Lofton, C.; Sigmund, W. *Adv. Funct. Mater.* **2005**, *15*, 1197.
(17) Elechiguerra, J. L.; Reyes-Gasga, J.; Yacamán, M. J. *J. Mater. Chem.* **2006**, *16*, 3906.
(18) Langille, M. R.; Zhang, J.; Personick, M. L.; Li, S.; Mirkin, C. A. *Science* **2012**, *337*, 954.
(19) Niu, W.; Zheng, S.; Wang, D.; Liu, X.; Li, H.; Han, S.; Chen, J.; Tang, Z.; Xu, G. *J. Am. Chem. Soc.* **2009**, *131*, 697.
(20) Sau, T. K.; Murphy, C. J. *J. Am. Chem. Soc.* **2004**, *126*, 8648.
(21) Personick, M. L.; Langille, M. R.; Zhang, J.; Harris, N.; Schatz, G. C.; Mirkin, C. A. *J. Am. Chem. Soc.* **2011**, *133*, 6170.
(22) Millstone, J. E.; Park, S.; Shuford, K. L.; Qin, L.; Schatz, G. C.; Mirkin, C. A. *J. Am. Chem. Soc.* **2005**, *127*, 5312.
(23) Jones, M. R.; Mirkin, C. A. *Angew. Chem., Int. Ed.* **2013**, DOI: 10.1002/anie.201209504.
(24) Millstone, J. E.; Métraux, G. S.; Mirkin, C. A. *Adv. Funct. Mater.* **2006**, *16*, 1209.
(25) Sun, Y.; Xia, Y. *Science* **2002**, *298*, 2176.
(26) Yin, Y.; Rioux, R. M.; Erdonmez, C. K.; Hughes, S.; Somorjai, G. A.; Alivisatos, A. P. *Science* **2004**, *304*, 711.
(27) Jiang, Q.; Jiang, Z.; Zhang, L.; Lin, H.; Yang, N.; Li, H.; Liu, D.; Xie, Z.; Tian, Z. *Nano Res.* **2011**, *4*, 612.
(28) Xue, C.; Mirkin, C. A. *Angew. Chem., Int. Ed.* **2007**, *46*, 2036.
(29) Xue, C.; Métraux, G. S.; Millstone, J. E.; Mirkin, C. A. *J. Am. Chem. Soc.* **2008**, *130*, 8337.
(30) Zhang, J.; Langille, M. R.; Mirkin, C. A. *J. Am. Chem. Soc.* **2010**, *132*, 12502.
(31) Millstone, J. E.; Hurst, S. J.; Métraux, G. S.; Cutler, J. I.; Mirkin, C. A. *Small* **2009**, *5*, 646.
(32) Wu, X.; Redmond, P. L.; Liu, H.; Chen, Y.; Steigerwald, M.; Brus, L. *J. Am. Chem. Soc.* **2008**, *130*, 9500.
(33) Aherne, D.; Ledwith, D. M.; Gara, M.; Kelly, J. M. *Adv. Funct. Mater.* **2008**, *18*, 2005.
(34) Zhong, J.; Qu, J.; Ye, F.; Wang, C.; Meng, L.; Yang, J. *J. Colloid Interface Sci.* **2011**, *361*, 59.
(35) Suzuki, K.; Hosokawa, K.; Maeda, M. *J. Am. Chem. Soc.* **2009**, *131*, 7518.
(36) Aubin-Tam, M.-E.; Hwang, W.; Hamad-Schifferli, K. *Proc. Natl. Acad. Sci. U.S.A.* **2009**, *106*, 4095.
(37) Métraux, G. S.; Cao, Y. C.; Jin, R. C.; Mirkin, C. A. *Nano Lett.* **2003**, *3*, 519.
(38) Sun, Y.; Xia, Y. *Adv. Mater.* **2003**, *15*, 695.
(39) Aherne, D.; Gara, M.; Kelly, J. M.; Gun'ko, Y. K. *Adv. Funct. Mater.* **2010**, *20*, 1329.
(40) Tian, N.; Zhou, Z.-Y.; Sun, S.-G.; Ding, Y.; Wang, Z. L. *Science* **2007**, *316*, 732.
(41) Ming, T.; Feng, W.; Tang, Q.; Wang, F.; Sun, L.; Wang, J.; Yan, C. *J. Am. Chem. Soc.* **2009**, *131*, 16350.
(42) Li, J.; Wang, L.; Liu, L.; Guo, L.; Han, X.; Zhang, Z. *Chem. Commun.* **2010**, *46*, 5109.
(43) Liu, M.; Guyot-Sionnest, P. *J. Phys. Chem. B* **2005**, *109*, 22192.
(44) Herrero, E.; Buller, L. J.; Abruña, H. D. *Chem. Rev.* **2001**, *101*, 1897.
(45) Oviedo, O. A.; Negre, C. F. A.; Mariscal, M. M.; Sánchez, C. G.; Leiva, E. P. M. *Electrochem. Commun.* **2012**, *16*, 1.
(46) Mariscal, M. M.; Oviedo, O. A.; Leiva, E. P. M. *J. Mater. Res.* **2012**, *27*, 1777.